Int J Mater Form
DOI 10.1007/s12289-017-1373-4

SI: MODELING MATERIALS AND PROCESSES, IN MEMORY OF PROFESSOR JOSÉ J. GRÁCIO

Incremental forming of Cu-35Zn brass alloy

Daniel Fritzen[1,2] · **Anderson Daleffe**[1] · **Gustavo do Santos De Lucca**[1] · **Jovani Castelan**[1] · **Lirio Schaeffer**[3] · **Ricardo J. Alves de Sousa**[2]

Received: 31 January 2017 / Accepted: 25 July 2017

Abstract Incremental Sheet Forming (ISF) and particularly its Single Point (SPIF) variant has been studied intensively over the last years given the potential for low-cost prototyping and small batches production. Numerical and experimental works have been covering a widespan of materials and geometries. This paper fills an important gap regarding studies of the SPIF process applied to brass alloys, and particularly the commonly used Cu-35Zn brass alloy. Despite being a material widely used in industry for centuries, with excellent cold formability and innumerous applications, there is still no relevant information on the mechanical response and properties of this material under SPIF. This research is based in SPIF experiments with brass alloy sheets with different thicknesses (0.50, 0.70 and 1.00 mm), to obtain data such as forming forces or forming fracture lines to be compared against standard forming limit diagrams or against other materials under ISF. Other data like friction during the process was evaluated as well. Fifteen sets of experiments were conducted, using different values of step down (0.10, 0.50 and 1.00 mm) and two forming tools with diameters 10 and 15 mm.

Keywords Incremental Sheet Metal Forming · Cu-35Zn Brass Alloy · Forming Forces · Friction

✉ Daniel Fritzen
daniel.fritzen@satc.edu.br

✉ Lirio Schaeffer
schaefer@ufrgs.br

✉ Ricardo J. Alves de Sousa
rsousa@ua.pt

[1] SATC University, Rua Pascoal Meller, 73 - Bairro Universitário - CEP, Criciúma, SC 88805-380, Brazil

[2] Center of Mechanical Technology and Automation-TEMA, Department of Mechanical Engineering, University of Aveiro, Campus Santiago, 3810-193 Aveiro, Portugal

[3] Metal Forming Laboratory –LdTM, Federal University of Rio Grande do Sul – UFRGS, Av. Bento Gonçalves 9500, CP 15021, Centro de Tecnologia – Campus da Agronomia, CEP, Porto Alegre, RS 91501-970, Brazil

Introdution

The incremental dieless forming process was described and patented by Lezak in 1967 [1], when CNC technology was still rudimentary. Only during in the 1990's, with the technological evolution of CNC equipment, the ISF research moved on, being widely studied and developed since then [2]. From few resources (backing plate, punch and a CNC machine), it is possible to form a series of products with different geometries, allowing great design flexibility at low expenses, becoming a competitive alternative to economically and efficiently produce small batches of formed products in sheet metal or other materials [3].

During the process, the sheet to be formed (blank) is clamped in a fixed support (backing plate). The simplest modality of ISF, is the Single Point Incremental Forming (SPIF). Figure 1 presents the basic components of the process; (i) the sheet metal blank, (ii) the blank holder, (iii) the backing plate and (iv) the rotating (actively or passively) forming tool [4]. A simple tool (cylindrical shank with the spherical/hemispherical tip) produces a small localized deformation on

Published online: 04 August 2017

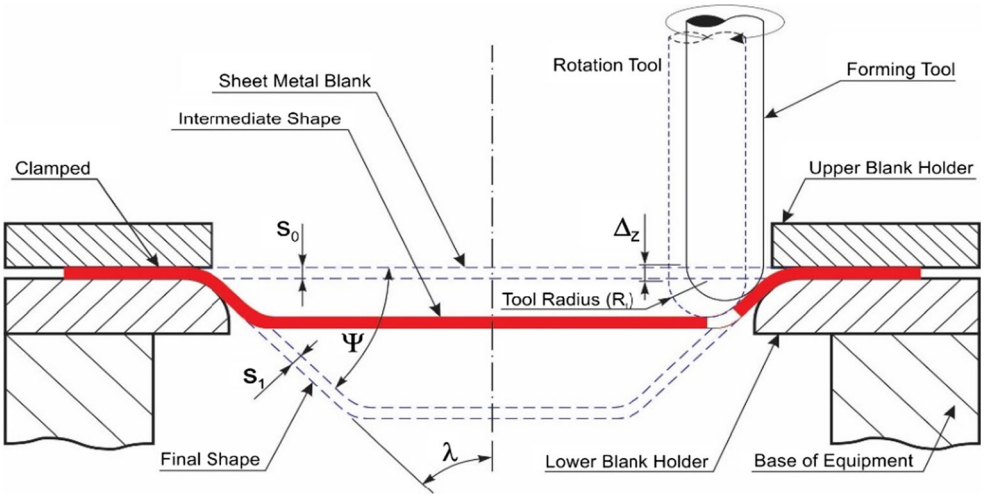

Fig. 1 Single Point Incremental Forming (SPIF) setup [4]

the sheet. Accordingly, the tool moves over the sheet, with gradual negative vertical increments (Δ_Z), deforming the new contact regions. Generally, the product to be manufactured and the tool deformation path are generated via CAD/CAM software [5].

The peculiar bending-stretch deformation mechanism during the forming operation contributes to a higher formability of the sheets [6], making it a very interesting process, especially for industries that require prototyping sheet metal, as the automotive and aerospace industries. There is a vast amount of research documented in literature over the last decades, dealing with numerical and experimental approaches and covering process forces, lubrication, materials, speed, material response, process parameters and others. Being impossible to cite all these works, the reader seeking for a proper introduction to ISF is suggested to check the state-of-art papers from Jeswiet and co-workers, from 2005 [3] and updated until 2015 [7], as well as the paper from Reddy *et al.* [8], where they report that recently the industry renewed its interest in ISF processes due to the change in consumer psychology, especially regarding the mass customization of products.

Much of the work carried out on ISF has been employing aluminium sheets, with several thickness, titanium and steel with moderate mechanical resistance and low sheet thickness values. Check reference [3] for the well-known review from Jeswiet et al., references [9–16] for references dealing mainly with aluminium and steel and [17] for titanium. Few works focused on high strength steels [18], being the reason linked to the machinery used: adapted milling machines or robots lack stiffness to promote high forming forces. With a different trend, brass alloys, a kind of material that shows moderate resistance, is compatible with some aluminium alloys but has receiving almost no attention from research groups. Few exceptions can be found in references [19] and [20] but even so, formability of brass alloys needs to be better characterized.

Brass and its alloys show excellent cold formality, good corrosion resistance and golden aspect, providing easy manufacturing of various products, such as core automotive radiators, heat exchangers, wind musical instruments and decorative parts. In fact, these characteristics and features seems to be a perfect match to ISF technology, focused on low batches and customized designs.

Continuing the preliminary researches conducted by Fritzen *et al.* [21], the objective of the work is to expand the range of materials employable within ISF, and to fill the evident gap regarding the study of brass material regarding its mechanical response. Summing up. this paper introduces the use of brass alloys in the ISF research, analysing the influence of sheet thickness (t_0), step down (Δ_Z), forming tool diameter (D_T), profile geometry and provides Forming Fracture Lines (FFL) to give an insight on the formability of this material.

Table 1 Chemical composition of brass alloy Cu – 35Zn [22]

Cu	Pb	Fe	Zn
64,00–68,50%	Max. 0,15%	Max. 0,05%	31,50–36,00%

Experimental tests

For this research, the Cu - 35Zn brass alloy (SAE J463) was chosen, belonging to the same group of cartridge brass (Cu - 30Zn), well-known for its excellent cold formability [22]. The

Table 2 Mechanical properties of brass alloy Cu – 35Zn [22]

Properties	Value
Density	8,47 g/cm^3
Young Modulus	105 GPa
Tensile Yield Stress	380 to 450 MPa
Hardness	132 HV

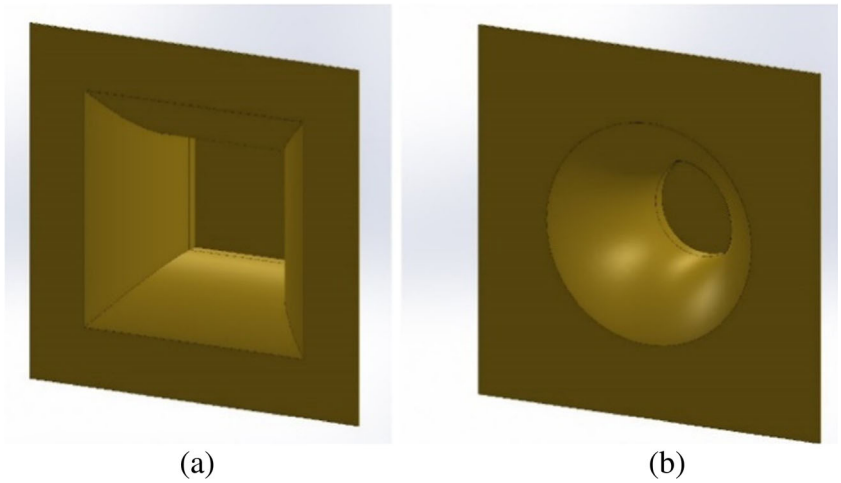

Fig. 2 Geometric profiles used in the experiments: (**a**) Pyramidal Frustums (**b**) Conical Frustums

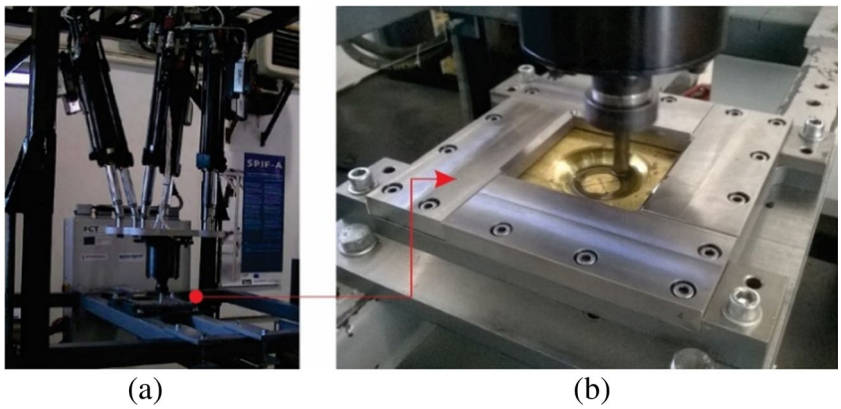

Fig. 3 (**a**) SPIFA machine; (**b**) Forming conical frustum Cu – 35Zn brass alloy

chemical composition is shown in Table 1 and their mechanical properties in Table 2.

To better characterize the materials prior to forming, tensile tests were carried out on a universal testing machine, model EMIC DL-10000, with 100kN capacity. Three tensile tests were carried out on 3 different direction (from rolling direction, 0°, 45° and 90°). To compute Forming Limit Diagrams (FLD), a hemispherical deformation punch test (Erischsen

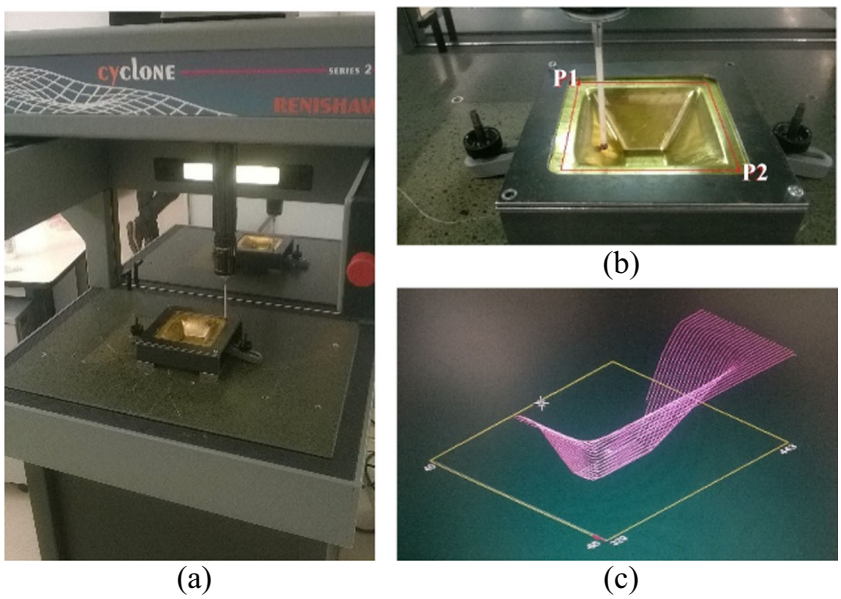

Fig. 4 Geometric Analysis: (**a**) CNC coordinate measurement machine; (**b**) Detail of contact probe and measuring area; (**c**) Three-dimensional file generated by measurement

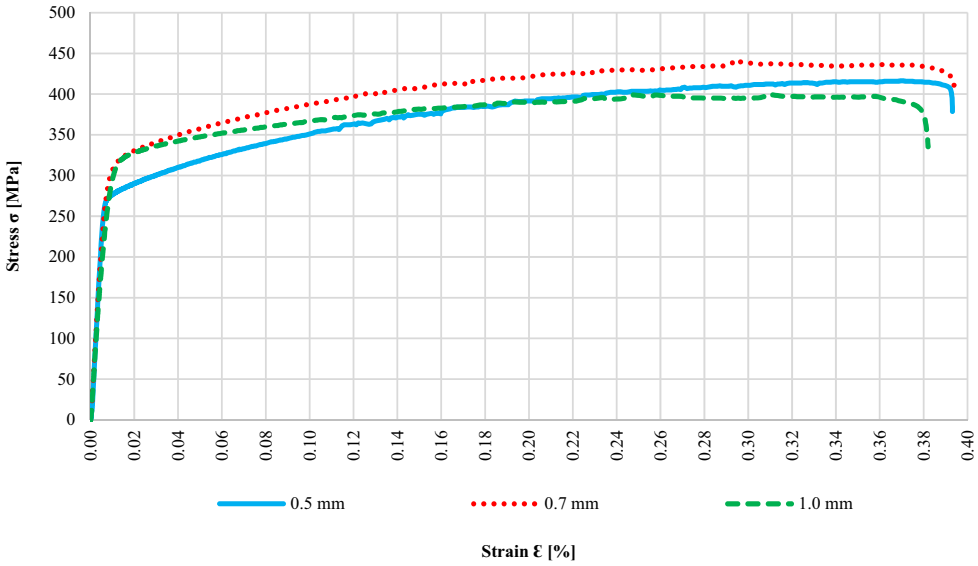

Fig. 5 Flow curve of Brass Alloy Cu-35Zn at rolling direction

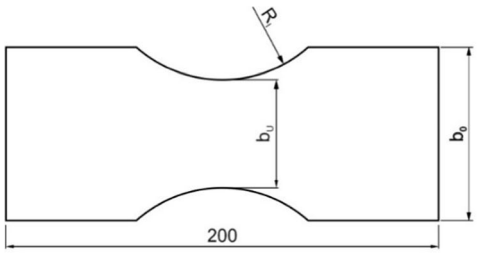

CP	R_i [mm]	b_u [mm]	b_0 [mm]
1	100	10	40
2	90	20	50
3	80	30	60
4	70	40	70
5	60	50	80
6	50	60	100
7	40	80	120
8	25	100	150

Fig. 6 Dimensions of the specimens (CP: Specimen number)

test) was employed, per ASTM E 2218–04. Both tests were performed on the three sheet thicknesses to be used with SPIF.

For SPIF experiments, conical and pyramidal frustums geometries were considered, according to the models used by Surresh and Regalla [16], in blanks of 150 mm × 150 mm, and 0.50, 0.70 and 1.00 mm thick (t_0), with radial profile wall (50 mm radius), diameter 100 mm and square 100 mm, respectively (Figure 2). The forming tool was also heat treated, resulting in an increased hardness to 58HRc. The tool geometry consists on a spherical tip with 10 and 15 mm diameter. The trajectory performed by the tool consists in the 3-axis contour tool path, with vertical increments (Δ_Z) of 0.10, 0.50 and 1.00 mm. The forming tool has passive rotation, as described in [3] and average travel velocity (feed rate) of 3000 mm/min. For the lubrication of the incremental forming process, mineral oil was used (Repsol SAE 30, [14]).

The 3D CAD models were made in SolidWorks® software, while the CNC program for ISF, in EdgeCAM® software. Although it is already proven in investigations about the SPIF process that the helical strategy is more adequate, because it decomposes the vertical Increment (Δ_Z) along all contour, and produces a better surface finish than the contour strategy [8], for the experiments of this investigation, the contour strategy – localized vertical Increment (Δ_Z) – was chosen to analyse the behaviour of the vertical force (F_Z) during the SPIF process.

The experiments were performed in the SPIF-A machine [23], developed specifically for incremental sheet forming (Figure 3). This machine has six independent degrees of freedom driven by hydraulic actuators. The machine withstands compressive and lateral loads and of 13 kN and 6.5 kN, respectively. The SPIF-A has three tri-axial load-cells placed between the spindle and mobile base of the Stewart platform.

To analyse the true strains (ε_1, ε_2), electrochemical etching was made using a grid of circles (Ø2,75 mm)

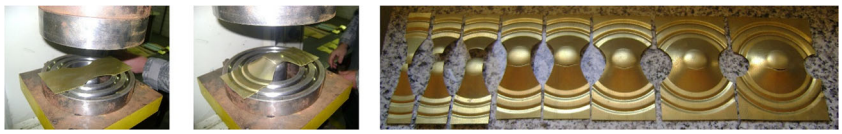

Fig. 7 Nakajima test and results

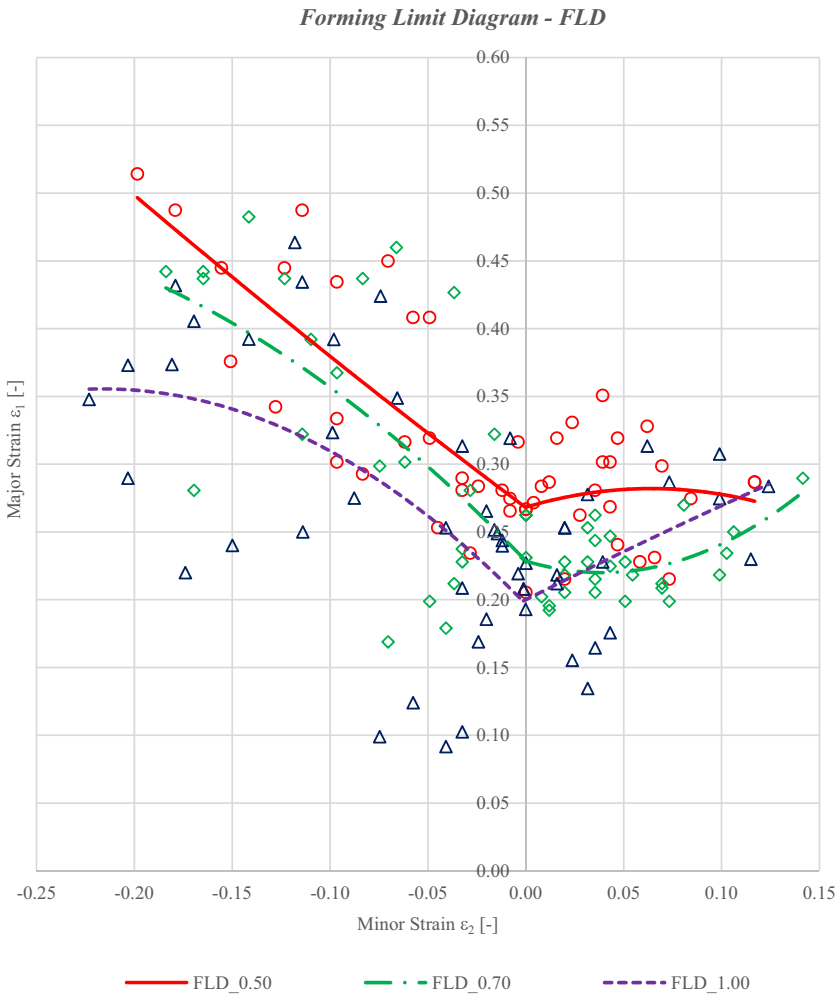

Fig. 8 FLD for different thickness of Cu-35Zn Brass Alloy

on the surface of each tested sheet. Measurements were performed with a digital stereoscope. The determination of the maximum wall angle (ψ) was carried out based on the maximum depth reached. For the analysis of the geometric profile, and consequently, the depth of fracture (D_P), a three-dimensional CNC coordinate measurement machine was used (Figure 4), Renishaw Cyclone Series 2, precision 0.005 mm. At the end of each measurement process, a CAD file (DXF) is generated (c), making possible the comparative analysis of the formed geometries against the designed one. In addition, the final thicknesses of the sheets were measured, using an external micrometer (Mitutoyo, resolution 0,01 mm). Finally, friction was computed as the ratio between radial and vertical forces, as in the classical sliding friction definition [14].

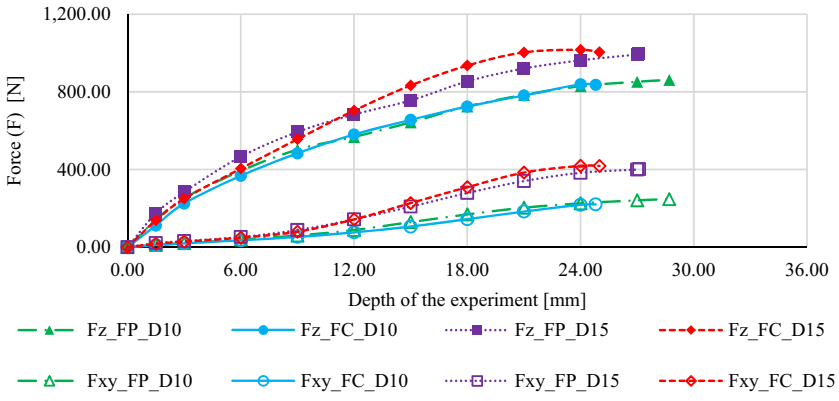

Fig. 9 Forming Force SPIF Brass: Δ_Z = 1.00 mm | t_0 = 0.50 mm

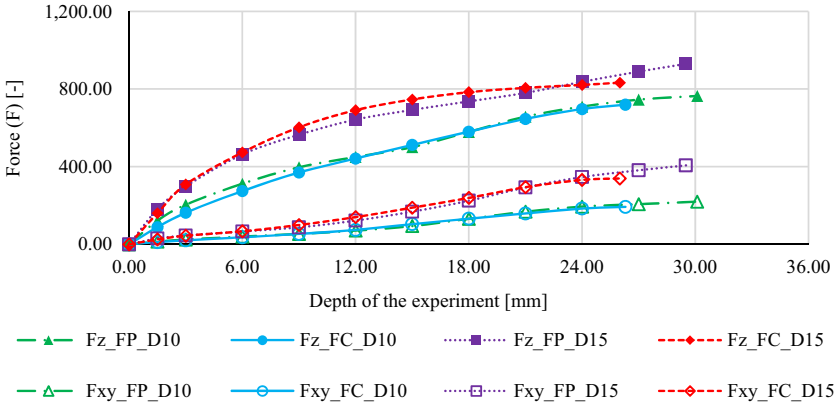

Fig. 10 Forming Force SPIF Brass: $\Delta_Z = 0.50$ mm | $t_0 = 0.50$ mm

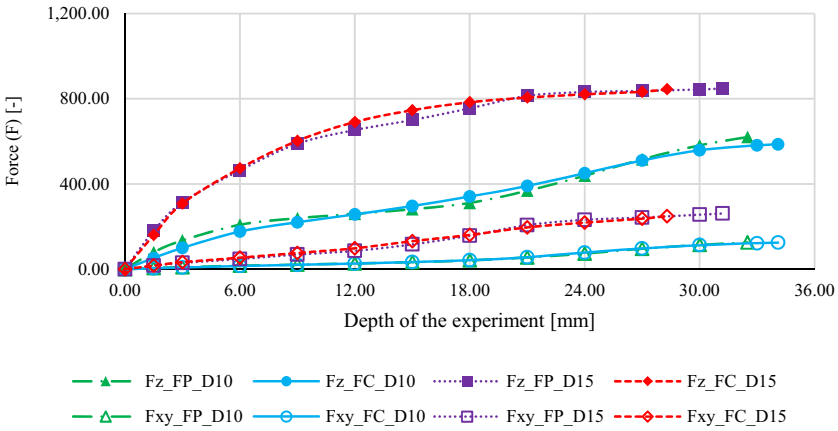

Fig. 11 Forming Force SPIF Brass: $\Delta_Z = 0.10$ mm | $t_0 = 0.50$ mm

Results

Characterization of the brass sheets

As an initial reference, Fig. 5 present the flow curve of Cu-35Zn Brass Alloy, for the 3 different thickness values under study. Rolling direction was considered. Peforming a fitting procedure using the Swift law ($\sigma = K\varepsilon^n$), yields hardening parameters n of 0.26, 0.22 and 0.19 for the 0.5 mm, 0.7 mm and 1.0 mm sheets respectively.

Forming Limit Diagrams were computed as well. Similarly, to tensile tests, FLDs were computed for 3 thickness values under study, Fig. 8. Computing a FLD begins with the experimental tests, where specimens with different widths are cut (Figure 6).

Then, the specimens are properly fixed in a backing plate and subjected to the hemispherical punch action until their rupture. The ε_1 *vs* ε_2 graphs were elaborated from the well-known procedure [24] based on Nakajima test (Figure 7).

The curves presented in Fig. 8 reveal a better formability for the thinner sheet (0.50 mm, $n = 0.26$) and a worse one for

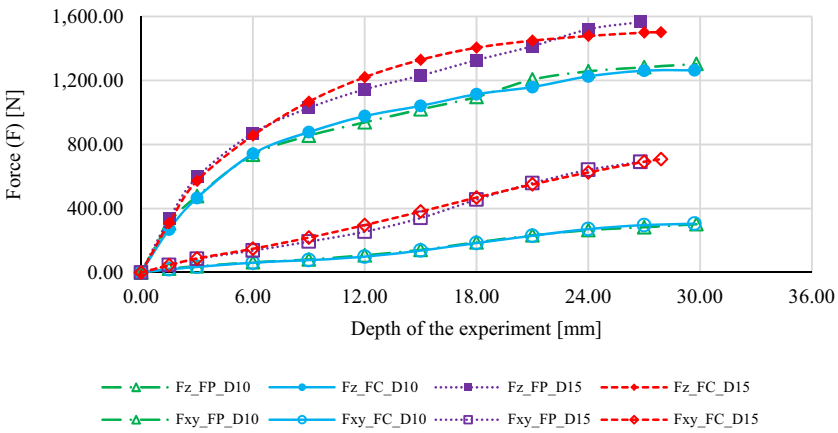

Fig. 12 Forming Force SPIF Brass: $\Delta_Z = 1.00$ mm | $t_0 = 0.70$ mm

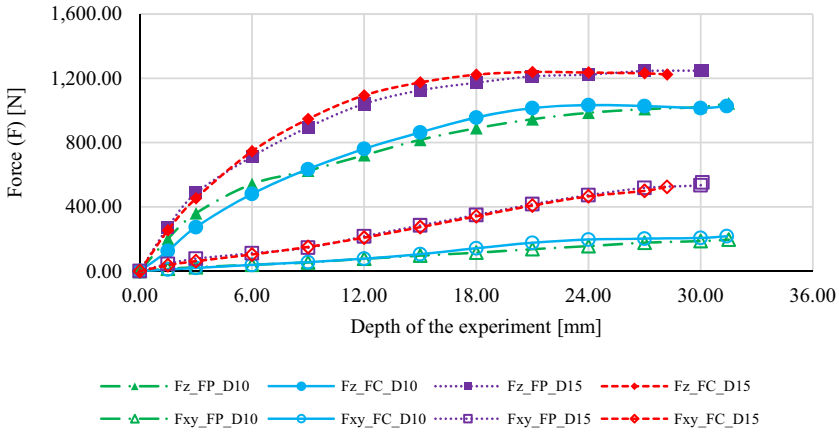

Fig. 13 Forming Force SPIF Brass: $\Delta_Z = 0.50$ mm | $t_0 = 0.70$ mm

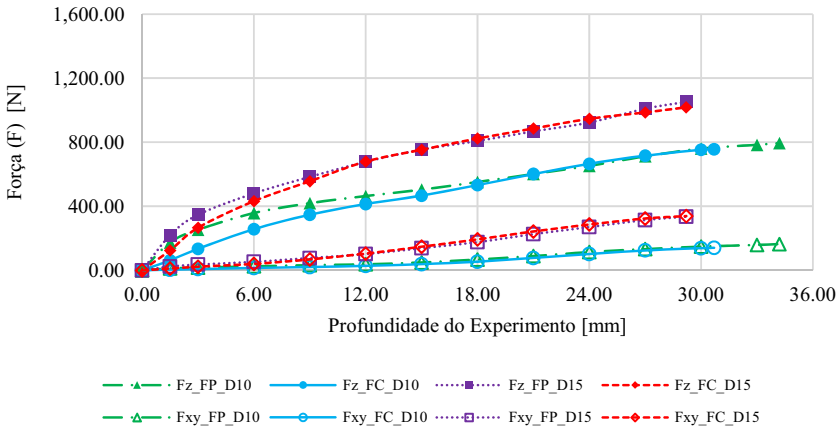

Fig. 14 Forming Force SPIF Brass: $\Delta_Z = 0.10$ mm | $t_0 = 0.70$ mm

the thicker (1.00 mm, $n = 0.19$), which comes in agreement with the computed flow curves (higher "n"parameter for the 0.5 mm sheet).

Despite the undeniable utility of FLDs under conventional press-forming, they reveal inefficient for incremental forming operation, given the diffuse necking phenomenon prior to fracture [4]. For this reason, Fracture Forming Lines (FFL) were computed and presented in "Forming Forces of Brass Alloy Sheets with SPIF" section.

Forming forces of brass alloy sheets with SPIF

Using the referred SPIF-A machine and the two proposed geometries, forming forces were acquired using 3D load cells. Compressive, vertical (F_Z), and radial, resultant on XY plane (F_{XY}) are presented with the following results (Figs. 9, 10, 11, 12, 13, 14, 15, 16 and 17). For easier inspection, data is organized and presented considering step down (Δ_Z) and sheet thickness (t_0). The following abbreviations also apply:

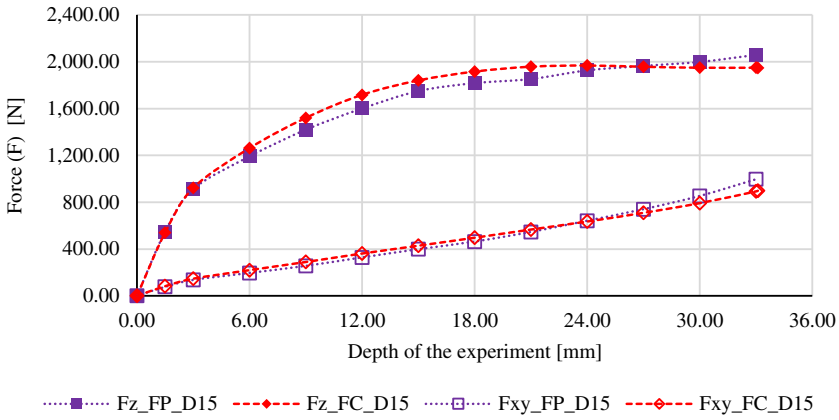

Fig. 15 Forming Force SPIF Brass: $\Delta_Z = 1.00$ mm | $t_0 = 1.00$ mm

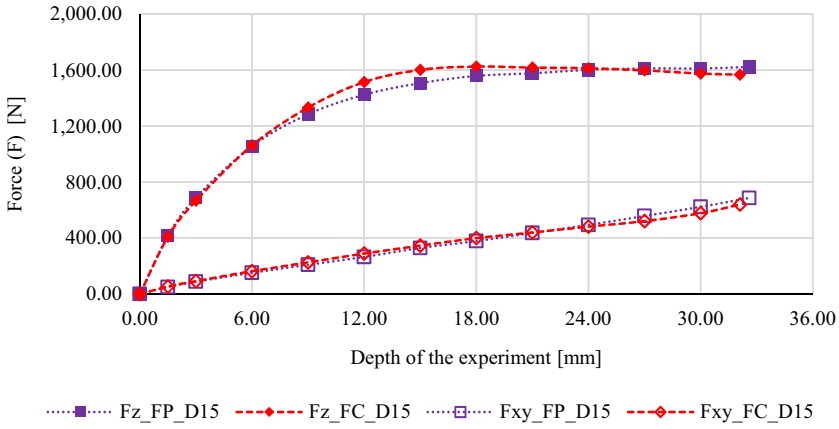

Fig. 16 Forming Force SPIF Brass: $\Delta_Z = 0.50$ mm | $t_0 = 1.00$ mm

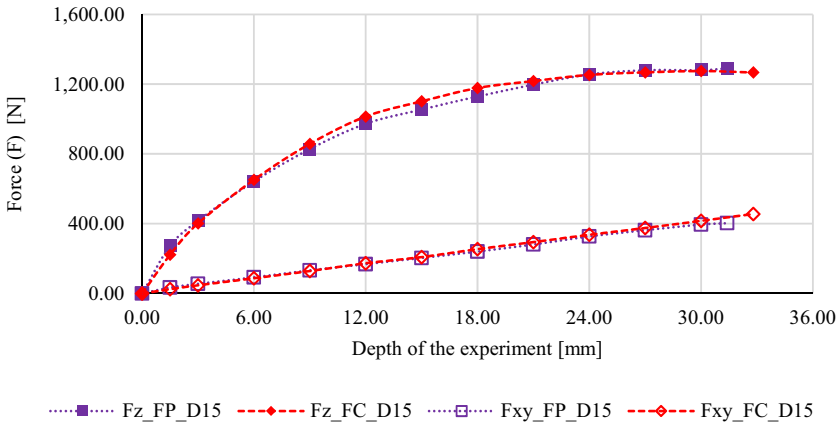

Fig. 17 Forming Force SPIF Brass: $\Delta_Z = 0.10$ mm | $t_0 = 1.00$ mm

- F_Z and F_{XY} refers to the measured force component;
- FC and FP refers to the geometry: Frustum: Conical and Frustum: Pyramidal, respectively;
- D10 and D15 refers to the forming tool diameter (D_T);

From the results presented from Fig. 9, 10, 11, 12, 13, 14, 15, 16 and 17 it can be inferred a similar trend for F_Z and F_{XY} components, i.e., they increase along with the forming depth (and consequently higher wall angle), for both geometries studied.

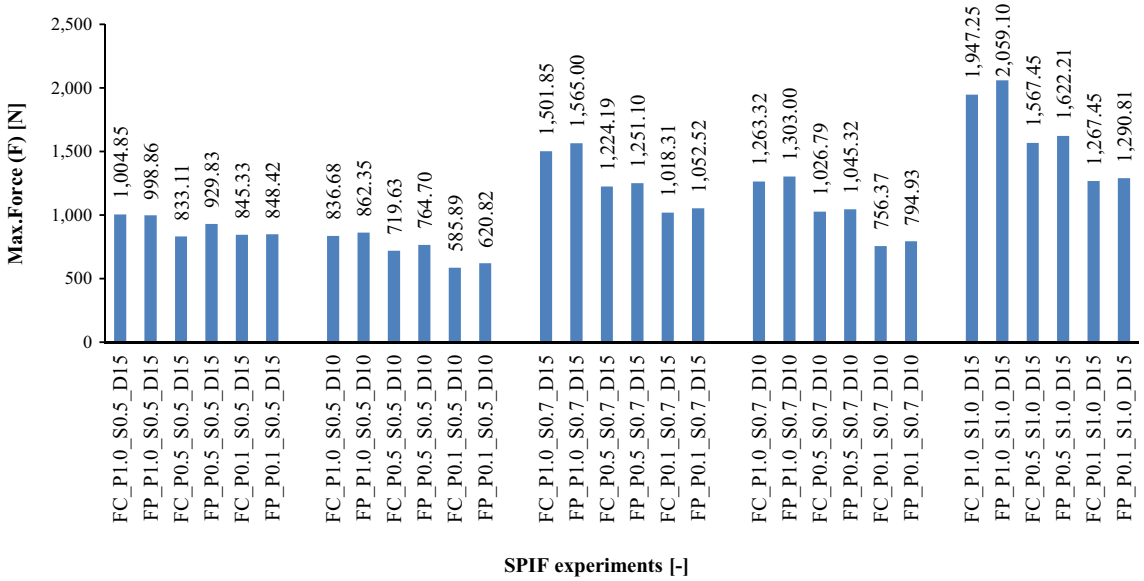

Fig. 18 All Forming Forces SPIF Brass

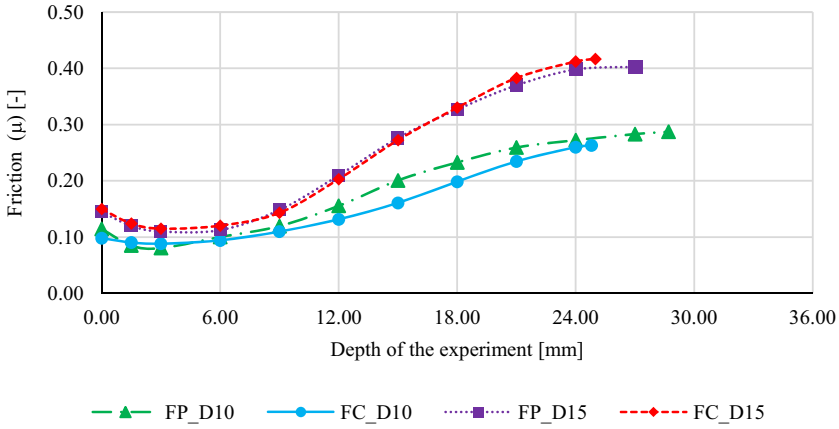

Fig. 19 Friction SPIF Brass: Δ_Z = 1.00 mm | t_0 = 0.50 mm

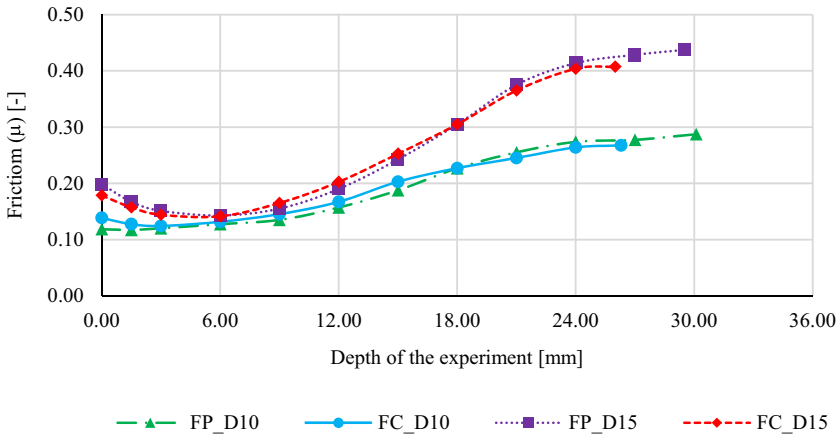

Fig. 20 Friction SPIF Brass: Δ_Z = 0.50 mm | t_0 = 0.50 mm

Additionally, it is also possible to observe smaller force (F_Z and F_{XY}) values in the experiments with smaller tool tip (Ø10 mm). In fact, the smaller the tool, the more localized is the deformation. According to Martins *et al.* [4], as the diameter of the forming tool increases, the more similar is the mechanical response under ISF with the conventional forming process.

In Azevedo *et al.* [14] researches, the Forces (F_Z and F_{XY}) of two different materials are analysed, the AA1050 aluminium alloy and DP780 steel alloy, both with 1 mm thickness, and although there is a great difference in the collected forces (350 N and 1500 N, respectively), there is similarity in the curves' trend. Curves obtained from the brass sheets are similar, showing that brass has a compatible response.

To illustrate the magnitude of Vertical Forces (F_Z) in SPIF process, Fig. 18 shows the maximum values of forces analysed at each experiment, separated according to their thicknesses.

The two geometric forms analysed showed similarity in the maximum values of Vertical Forces (F_Z). Also, it is observed that the maximum forces decrease for smaller step down (Δ_Z) values.

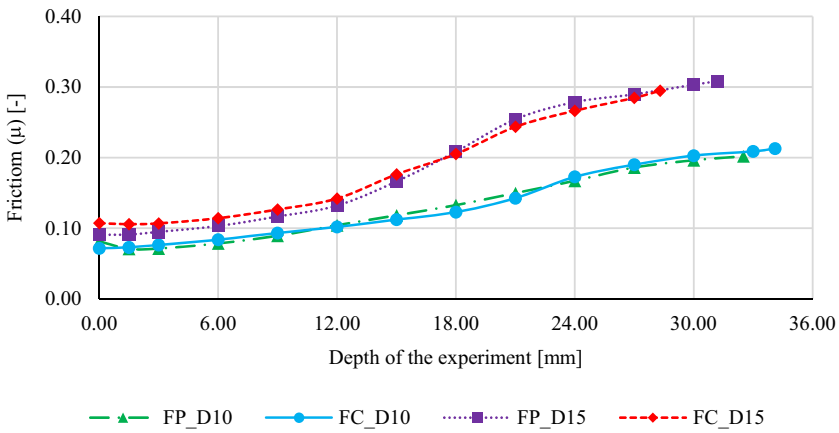

Fig. 21 Friction SPIF Brass: Δ_Z = 0.10 mm | t_0 = 0.50 mm

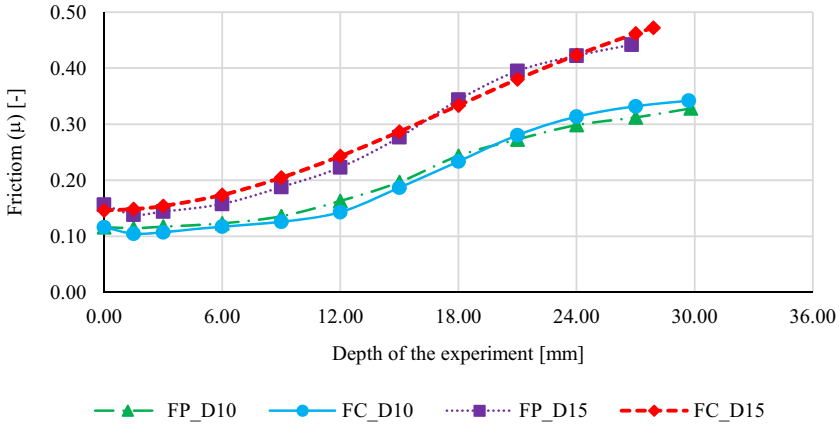

Fig. 22 Friction SPIF Brass: $\Delta_Z = 1.00$ mm | $t_0 = 0.70$ mm

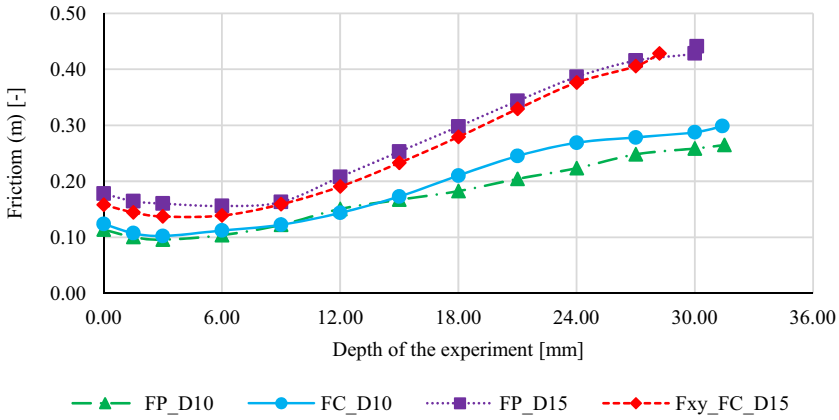

Fig. 23 Friction SPIF Brass: $\Delta_Z = 0.50$ mm | $t_0 = 0.70$ mm

Following the same form of organization of the force results, friction effects (μ) are presented from Figs. 19, 20, 21, 22, 23, 24, 25, 26 and 27.

Since the friction values (μ) are calculated in function of the Forces (F_Z and F_{XY}). Naturally, friction values (μ) coming from the Ø15 mm forming tool experiments are greater than the Ø10 mm tool ones, once the contact area is larger.

A relation between the friction value (μ) and the initial sheet thickness (t_0) is verified. In fact, for the higher thicknesses (1.0 mm), the friction evolution during the process is roughly monotonically crescent, almost linear. As sheet thickness goes to 0.5 mm and 0.7 mm such evolution tends to be non-linear.

Formability and geometrical accuracy

All measurements from SPIF made geometries were performed at the rolling direction (0°). Figure 28 compares the measured profiles against the CAD geometry.

Geometrical inaccuracy is still one of the major drawbacks in ISF operations. Based on Fig. 28, it is observed that none of

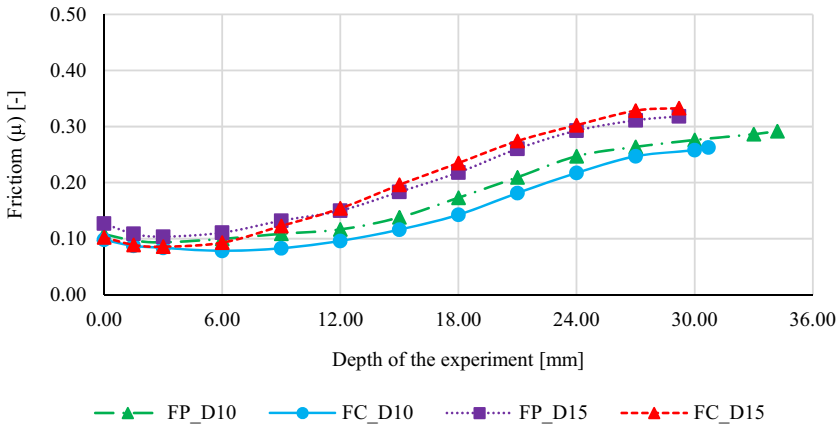

Fig. 24 Friction SPIF Brass: $\Delta_Z = 0.10$ mm | $t_0 = 0.70$ mm

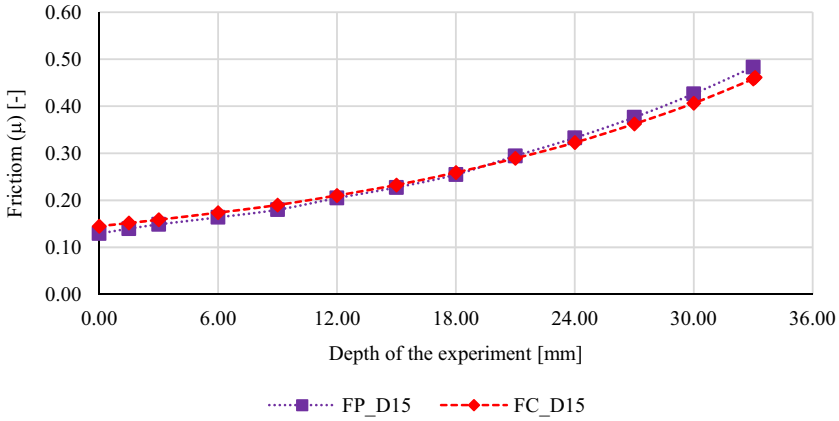

Fig. 25 Friction SPIF Brass: $\Delta_Z = 1.00$ mm | $t_0 = 1.00$ mm

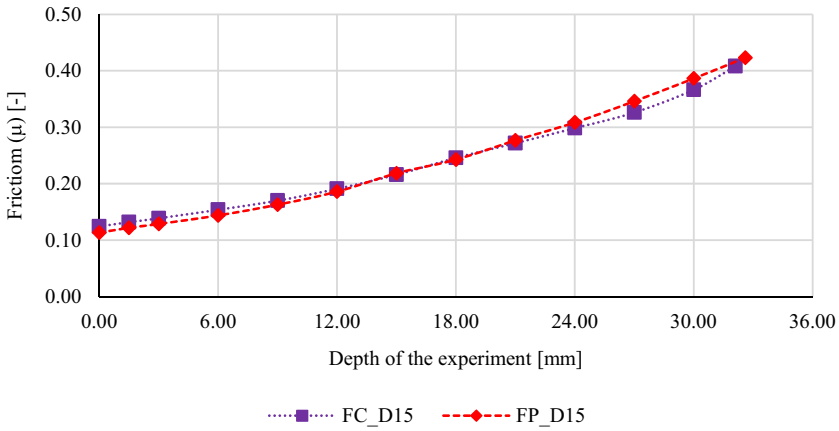

Fig. 26 Friction SPIF Brass: $\Delta_Z = 0.50$ mm | $t_0 = 1.00$ mm

the SPIF profiles measured match the designed part. All of them show geometrical deviations.

Such deviations corroborate with Allwood *et al.* [25] (or many other authors), where it is reported that acceptable dimensional tolerances for sheet metal components are normally ±0.2 mm, however for conventional ISF processes dimensional accuracy is only ±3 mm. Another fact refers to the depths reached on each SPIF experiment. According to Martins *et al.* [4], the use of forming tools with smaller diameter (D_T) provides better formability because the stress concentrations are in a smaller region of deformation of the sheet. In Fig. 27 is possible to observe that the experiments with tool Ø10 mm obtained the greatest depths, as also observed by Centeno *et al.* [13].

At the lateral flaps, restrained during forming operation by the blank holder, there was a significant amount of deformation. Allwood *et al.* [25] and Ambrogio *et al.* [26] described this behaviour of the sheet as resulting from the accumulation (and relaxation) of residual stresses, appearing after the release of the blank holder.

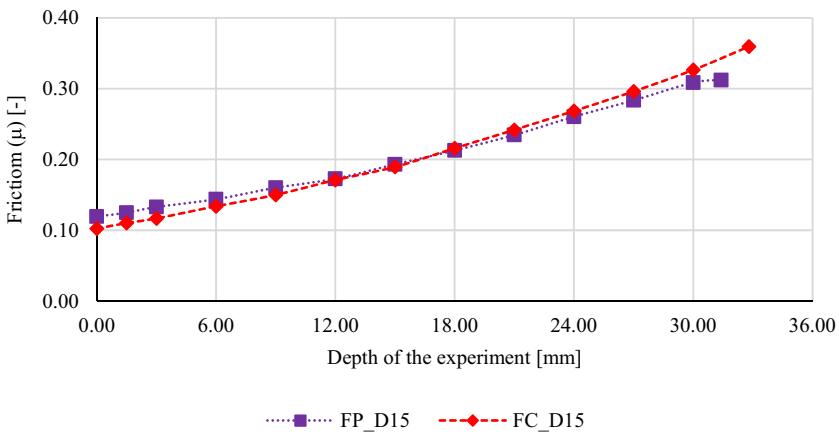

Fig. 27 Friction SPIF Brass: $\Delta_Z = 0.10$ mm | $t_0 = 1.00$ mm

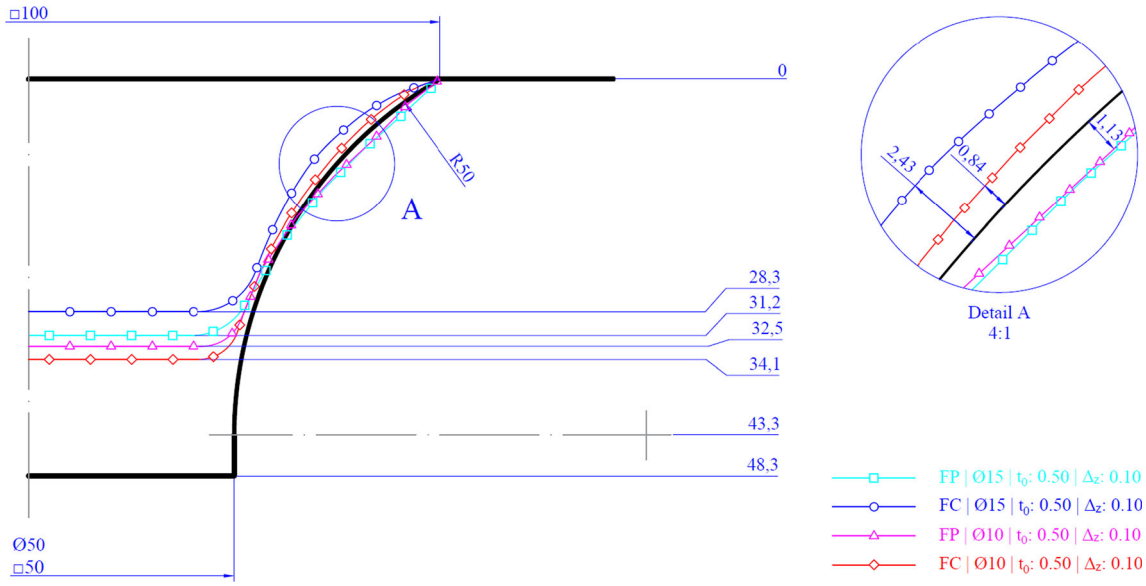

Fig. 28 SPIF experiments geometric profiles: t_0: 0,50 mm | Δ_Z: 0,10 mm

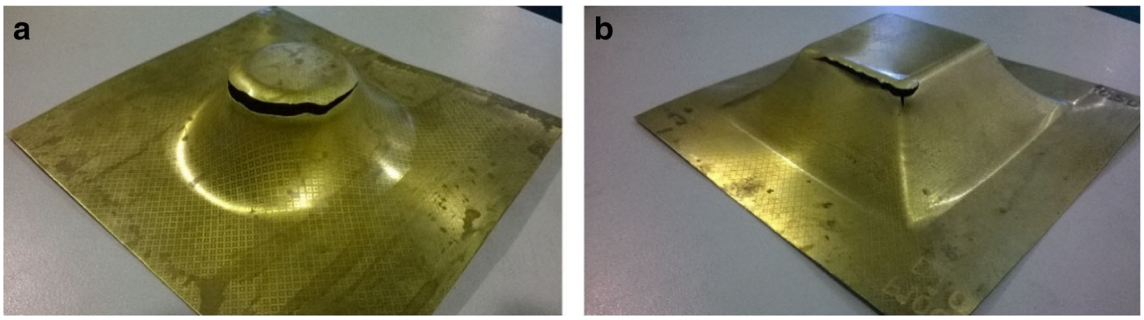

Fig. 29 SPIF experiments: (**a**) Conical Frustum, (**b**) Pyramidal Frustums [t_0: 0.50 mm| Δ_Z: 1.00 | Ø10 mm]

All the experiments performed suffered a fracture in the same region, which lays in the contact zone of the tool with the sheet. Figure 29 shows two fractured SPIF experiments. Once fracture is initiated, and given the diffuse necking and high stress concentration, it quickly spreads.

The results of all SPIF experiments performed, with respect to the fracture depths (D_F) and the respective Wall Angles (Ψ) can be seen in Table 3.

Analysing Table 3 data, it is observed that most of experiments follow the usual trends in SPIF, when a smaller step

Table 3 Wall Angle (Ψ) values and maximum depths of the SPIF experiments

t_0 [mm]	Δ_Z [mm]	Ø15				Ø10			
		Conical Frustum		Pyramidal Frustum		Conical Frustum		Pyramidal Frustum	
		D_F [mm]	Ψ [°]	D_F [mm]	Ψ [°]	D_F [mm]	Ψ [°]	D_F [mm]	Ψ [°]
0.50	0.10	28,30	66,90	31,20	70,10	34,10	75,10	32,50	73,20
	0.50	26,00	64,40	29,50	68,30	26,30	66,40	30,10	70,70
	1.00	25,00	63,30	27,10	65,70	24,80	64,70	28,70	69,10
0.70	0.10	29,20	67,90	29,20	67,90	30,70	71,40	34,20	75,10
	0.50	28,20	66,90	30,10	68,90	31,40	72,10	31,50	72,30
	1.00	27,90	66,50	26,80	65,30	29,70	70,30	29,80	70,30
1.00	0.10	32,80	71,80	31,40	70,30	-	-	-	-
	0.50	32,10	71,00	32,60	71,50	-	-	-	-
	1.00	33,10	72,10	33,00	72,00	-	-	-	-

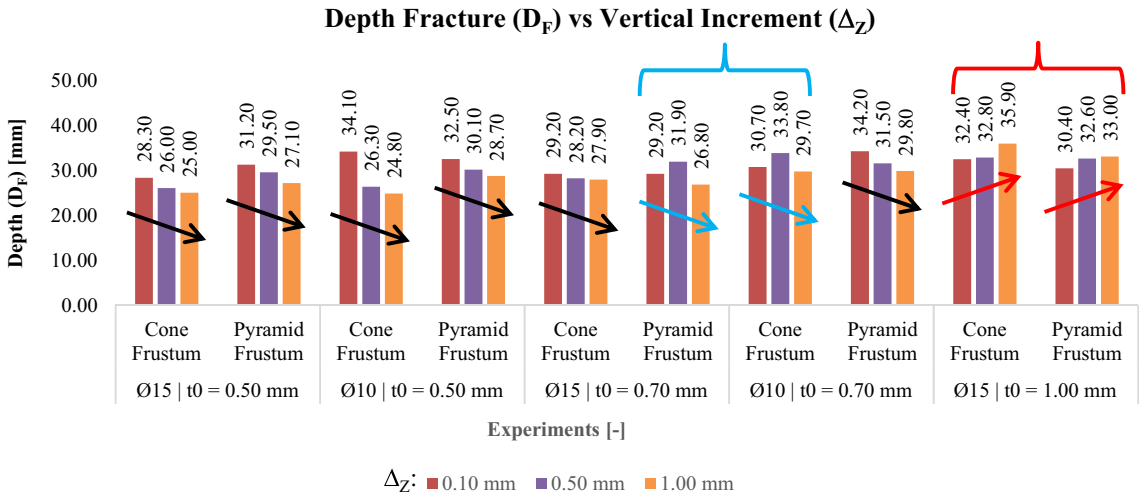

Fig. 30 Values of maximum depths reached in all experiments

down (Δ_Z) leads to higher depths and wall angles, corroborating [4, 13]. Figure 30 translate the previous table into a graphical form.

It is possible to check that four experiments do not follow the usual tendency. In the set of experiments 06 (t_0: 0.70 mm | Ø15 mm | Pyramidal Frustum) the higher depth is observed for a 0.50 mm step down. The same was observed in experiments 07 (t_0: 0.70 mm | Ø10 mm | Conical Frustum). Since experiments number 06 (Pyramid) and number 05 (Cone) were performed under the same parameters, such differences might be related with the distinct geometries performed.

Finally, an inverted max. Depth evolution is observed for experiments number 09 (t_0: 1.00 mm | Ø15 mm | Conical Frustum) and number 10 (t_0: 1.00 mm | Ø15 mm | Pyramidal Frustum), where higher depths were obtained with the higher step-down of 1.00 mm.

The final thicknesses (t_1) of each experiment were also analysed, to verify the validity of the Sine Law during SPIF with brass alloys. Figure 31 shows the lowest final thickness values (t_1) measured (near the fractured region in the formed area) compared to the values calculated by Sine Law, as a function of the Wall Angle (Ψ), listed in Table 3.

Naturally, analysing the data on Fig. 31, it is noticed that the lower the initial thickness (t_0) of the sheet, the lower variation of the measured and calculated values. In fact, the higher the thickness, the higher will be forming forces, shear strains and resulting stresses, which will lead to more pronounced deviations. Table 4 groups the values according to

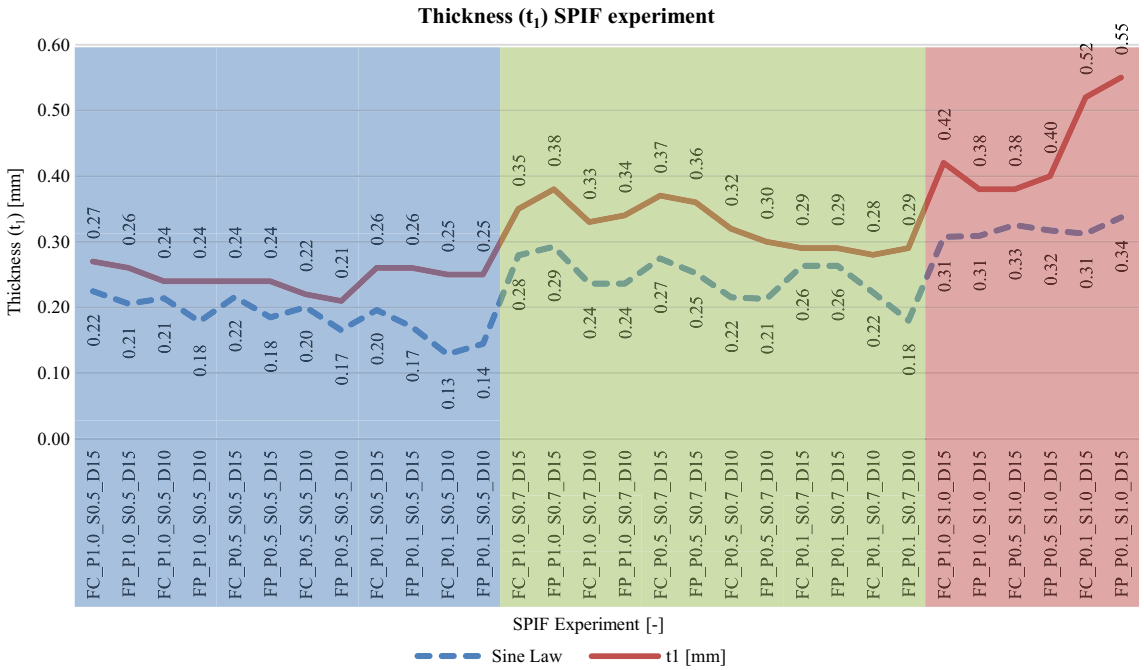

Fig. 31 Lower values of final thickness (t_1) measured in the experiments

Table 4 Values of the Sine Law and the values measured in the final thickness (t_1) of the sheet

t_0 [mm]	Sine Law [mm]			s_1 [mm]		
	Average value	Standard deviation	Thickness reduction	Average value	Standard deviation	Thickness reduction
0,50	0,19	0,03	62,86%	0,25	0,02	51,00%
0,70	0,24	0,03	65,14%	0,33	0,04	53,57%
1,00	0,32	0,05	68,19%	0,44	0,07	55,83%

the initial thickness of the sheets. The values calculated by the Sine Law point to a reduction of 62% to 68% of the thickness of the sheet, while for the measured values is between 51% and 55%.

Finally, Fracture Forming Lines were elaborated, after analysing the deformations (ε_1 and ε_2) of the circle grid (turned into ellipses) near the fractured regions, for the variety of geometries studied, including not only frustrum-type geometries, but also constant slope cones and pyramids, With the measurement of the ellipses in the SPIF experiments, it was observed that the calculated values of the deformations (ε_1 and ε_2) are very close, independent of the forming tool diameter (D_T). Contrarily, the Vertical Increment (Δ_z) yields different fracture lines.

Figure 32 shows the analysed deformations of SPIF experiments with t_0: 0.50 mm thickness, respective FFLs and FLD for comparison purposes.

As reported for instance by Jeswiet *et al.* [3], the smaller the step down (Δ_z) used in the ISF process, the greater the material formability in ISF. Figure 32 portrays precisely this aspect, where the major strain for 0.10 mm step down is circa 0,75, while for 1.00 mm, is reduced to 0,63, but still higher than in the FLD. Figure 33 shows the analysed deformations of SPIF experiments with t_0: 0.70 mm thickness.

In Fig. 33, the same behaviour of the resulting FFL is observed, with the highest deformations corresponding to the lowest step down (Δ_Z = 0.10 mm), and in this case, with similar values to the FFL of Fig. 32. The FFL with step down 1.00 mm is slightly below the FFL of Fig. 32, while the FFL with the step down of 0.50 mm slightly higher.

Figure 34 shows the analysed deformations of SPIF experiments with t_0: 1.00 mm thickness.

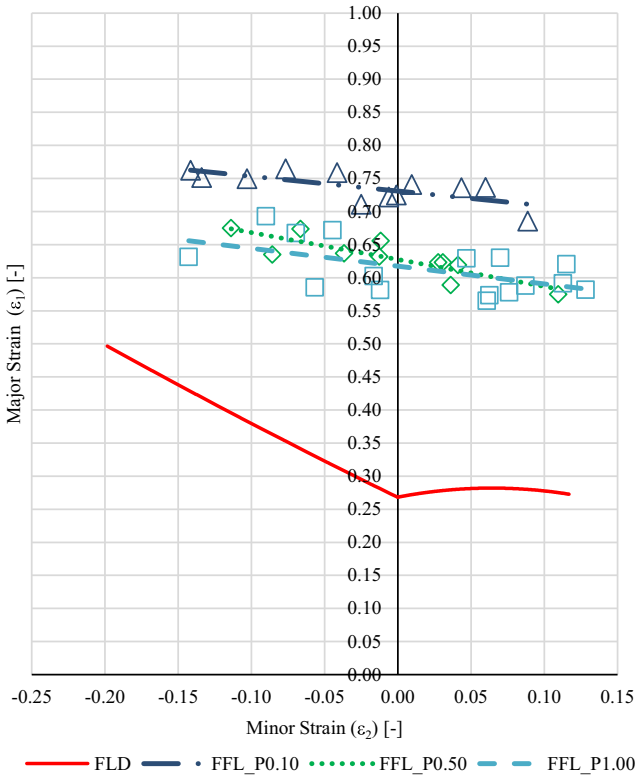

Fig. 32 Fracture Forming Lines (t_0: 0,50 mm)

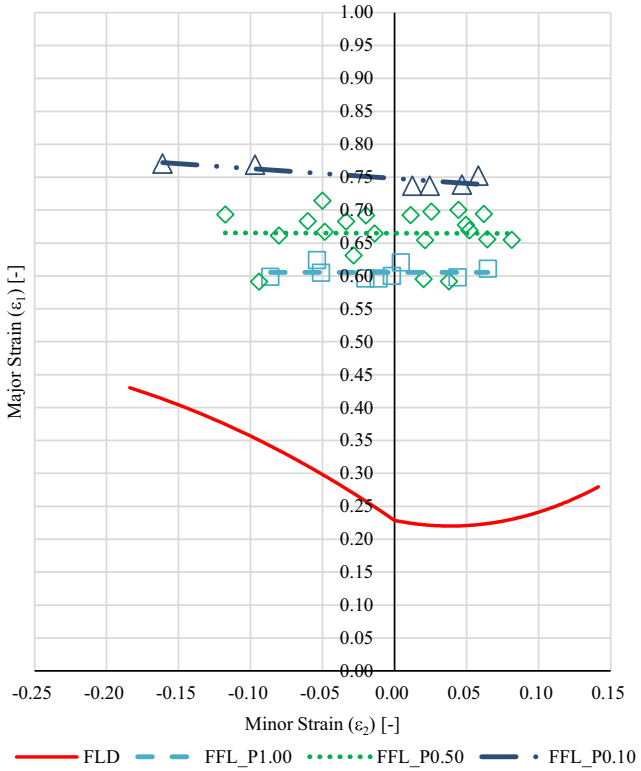

Fig. 33 Fracture Forming Line (t_0: 0.70 mm)

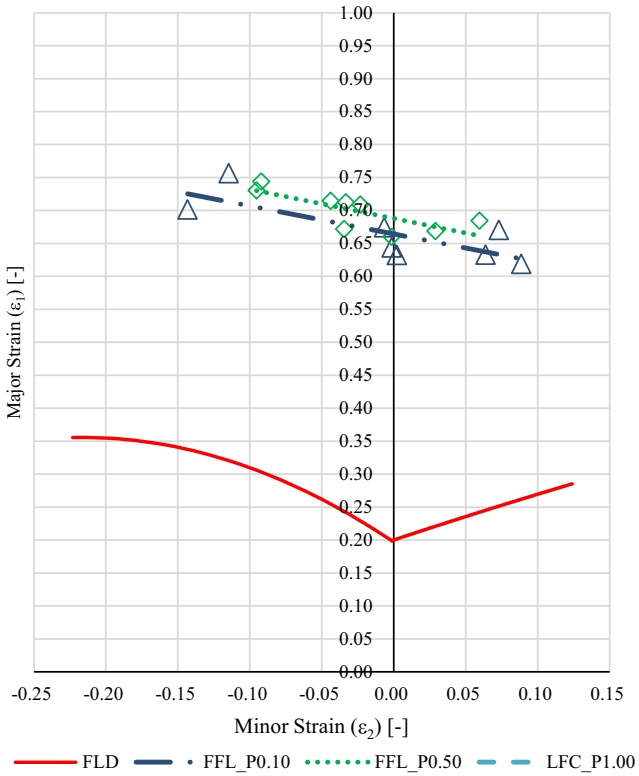

Fig. 34 Fracture Forming Line (t_0: 1.00 mm)

Similarly, to previous FFLs, the smallest step down produces the largest deformations. However, for this 1.00 mm thick brass sheet, the influence of step down is clearly reduced. Hence, the thicker the sheet the lower the beneficial effect of step-down in formability.

Common to all FFL graphs is the clear formability improvement when compared to FLD for the same thickness. So, the improved formability of ISF also hold for brass alloys.

The maximum values of major strain (ε_1) are close for the three thicknesses values studied, indicating a maximum deformation limit for this material (in these experimental configurations).

Conclusions

Currently, research on incremental forming technology has been focusing more usually on aluminium material, and also on steel and titanium alloys.

This work focused on brass alloys, a noble material, that despite being pricey, is traditionally applied in decoration, ornaments or custom made parts. In this sense, ISF technology has a huge potential to shape brass sheets at an affordable price for customized products.

The experiments showed that the brass alloy studied showed a regular, expected performance under SPIF when compared with other already documented materials. In this sense, formability is increased with the FFL appearing above than the conventional FLC of the material. The formability improvement is more pronounced for smaller tool diameters, a phenomenon also reported in literature for other materials. Doing so, the highest wall angles for the 2 geometries studied were obtained for the 10 mm diameter tool. Regarding wall thickness reduction, the sine law was fairly followed. In the studied cases, the law pointed for thickness reduction between 62% and 68% but the measured values situated between 51% and 55%. Forming forces were kept at acceptable levels and evolving like expected on SPIF operations.

Regarding ISF processing parameters, it can be inferred a significant effect of step down size. Like other materials, higher step down sizes will imply large forming forces and worse surface finish. Likewise, higher sheet thicknesses and larger tool diameters will increase forming forces. Dimensional inaccuracy is also a barrier for brass alloys under SPIF, with the measured formed geometries presenting deviations when compared to the designed CAD (± 3 mm), compatible to values reported in literature for aluminium. In this sense, much of work carried out by other groups regarding optimized toolpaths can be perfectly employed to brass materials.

Summing up, this paper documented the mechanical response of brass alloy sheets under incremental forming, filling a gap in the literature. The material shows compatible properties when compared to other types of materials commonly used in ISF and proves that brass alloys can be easily employed in this low batches, highly customizable technique.

Acknowledgments The authors thank National Council of Scientific Development – CNPq (Process 234851/2014-7) for financial support in developing this project; UFRGS/LdTM, University of Aveiro, Center of Mechanical Technology and Automation (TEMA), North Aveiro Polytechnic School (ESAN) and SATC University for technical and scientific support.

Compliance with ethical standards

Conflict of interest None.

References

1. Leszak E (1967, Setembro 19) Apparatus and Process for Incremental Dieless Forming. USA Patent US3342051A1
2. Behera AK, Alves de Sousa R, Ingarao G, Oleksik V (2017) Single point incremental forming: An assessment of the progress and technology trends from 2005 to 2015. J Manuf Process 27:37–62. htpps://doi.org/10.1016/j.jmapro.2017.03.014
3. Jeswiet J, Micari F, Hirt G, Bramley A, Duflou J, Allwood J (2005) Asymmetric Single Point Incremental Forming of Sheet Metal. CIRP Ann Manuf Technol 54(2):88–114
4. Martins PAF, Bay N, Skjoedt M, Silva MB (2008) Theory of single point incremental forming. CIRP Ann 57(1):247–252. https://doi.org/10.1016/j.cirp.2008.03.047

5. Hirt G,. Junk S, Bambach M, Chouvalova I, Ames J (2005) Flexible CNC Incremental Sheet Forming: Process Evaluation and Simulation. Institute of Materials Technology/Precision Forming (LWP), Saarland University, Germany, p 12
6. Emmens W, van den Boogaard A (2009) An overview of stabilizing deformation mechanisms in incremental sheet forming. J Mater Process Technol 209:3688–3695
7. Jeswiet J, Adams D, Doolan M, McAnulty T, Gupta P (2015) Single point and asymmetric incremental forming. Adv Manuf 3(4):253–262
8. Reddy NV, Lingam R, Cao J (2015) Incremental Metal Forming Processes in Manufacturing. Handbook of Manufacturing Engineering and Technology, pp. 411–452
9. Duflou J, Verbert J, Belkassem B, Gu J, Sol H, Henrard C, Habraken A (2008) Process window enhancement for single point incremental forming through multi-step toolpaths. CIRP Ann Manuf Technol 57:253–256
10. Ambrogio G, Filice L, Gagliardi F (2012) Formability of light-weight alloys by hot incremental sheet forming. Mater Des 34: 501–508
11. Araghi BT, Göttmann A, Bergweiler G, Saeed-Akbari A, Bültmann J, Zettler J, Bambach M, Hirt G (2011) Investigation on Incremental Sheet Forming Combined with Laser Heating and Stretch Forming for the Production of lightweight structures. Key Eng Mater 473: 919–928
12. Castelan J, Daleffe A, Schaeffer L, Casagrande J, Gruber V, Fritzen D (2010) Development of Cranial Implant Through Incremental Sheet Forming for Medical Orthopedic Applications. Int J Mater Eng Technol 4(1):63–80
13. Centeno G, Bagudanch I, Martínez-Donaire A, García-Romeu ML, Vallellano C (2014) Critical Analysis of Necking and Fracture Limit Strains and Forming Forces in Single-Point Incremental Forming. Mater Des 63:20–29
14. Azevedo NG, Farias JS, Bastos RP, Teixeira P, Davim JP, Sousa RJA (2015) Lubrication Aspects during Single Point Incremental Forming for Steel and Aluminum Materials. Int J Precis Eng Manuf 16(3):1–7
15. Minutolo F, Durante M, Formisano A (2007) Evaluation of the maximum slope angle of simple geometries carried out by incremental forming process. J Mater Process Technol 194:145–150
16. Suresh K, Regalla S (2014) Analysis of formability in single point incremental forming using finite element simulations. Procedia Mater Sci 6:430–435
17. Daleffe A, Schaeffer L, Fritzen D, Castelan J (2013) Analysis of the Incremental Forming of Titanium F67 Grade 2 Sheet. Key Eng Mater 554-557:195–203
18. Bastos R, Sousa R, Ferreira J Enhancing time efficiency on single point incremental forming processes. Int J Mater Form 9(5):653–662. https://doi.org/10.1007/s12289-015-1251-x
19. Kumar Y, Kumar S (2015) Incremental Sheet Forming (ISF). Advances in Material Forming and Joining, pp 29–46. https://doi.org/10.1007/978-81-322-2355-9_2
20. Al-Attaby Q, Abaas T, Bedan A (2013) The Effect of Tool Path Strategy on Mechanical Properties of Brass (65-35) in Single Point Incremental Sheet Metal Forming (SPIF). J Eng 19(5):629–637
21. Fritzen D, De Lucca GS, Marques FM, Daleffe A, Castelan J, Boff U, Sousa RJAD, Schaeffer L (2016) SPIF of Brass alloys: Preliminary studies. AIP Conf Proc 1769:060006. https://doi.org/10.1063/1.4963442
22. ASM I (1992) ASM HANDBOOK - Properties and Selection: Nonferrous Alloys an Special-Purpose Materials, vol 2. ASM INTERNATIONAL, USA, p 3470
23. Sousa R, Ferreira J, Sa de Farias J, Torrao J, Afonso D, Martins M (2014) SPIF-A: on the development of a new concept of incremental forming machine. Struct Eng Mech 49(5):645–660
24. ASTM E2218-02 (2002) Standard Test Method For Determining Forming Limit Curves. ASTM International, West Conshohocken, PA. https://www.astm.org
25. Allwood J, Braun D, Music O (2010) The effect of partially cut-out blanks on geometric accuracy in incremental sheet forming. J Mater Process Technol 210:1501–1510
26. Ambrogio G, De Napoli L, Filice L, Gagliar F, Muzzupappa M (2005) Application of Incremental Forming process for high customised medical product manufacturing. J Mater Process Technol 162:156–162. https://doi.org/10.1016/j.jmatprotec.2005.02.148
27. Bagudanch I, Centeno G, Vallellano C, Garcia-Romeu ML (2013) Forming force in Single Point Incremental Forming under different bending conditions. Manuf Eng Soc Int Conf MESIC 63:354–360
28. A. Blaga (2011) Contributions to the incremental forming of thin metal sheets. PhD Thesis, University Lucian Blaga din Sibiu, Sibiu, p. 78